

# Millimeter-wave Channel-Sounder Performance Verification using Vector Network Analyzer in a Controlled RF Channel

Jeanne T. Quimby, *Member, IEEE*, Dylan F. Williams, *Fellow, IEEE*, Kate A. Remley, *Fellow, IEEE*, Diogo Ribeiro, Ruoyu Sun and Jelena Senic

**Abstract**—A new comparison-to-reference performance verification technique compares an E-band channel-sounder and reference vector network analyzer measurements of the same controlled, static channel. This new technique reduces the number of inaccurate assumptions that exist in other methods providing a stronger verification of the channel-sounder hardware and processing performance. This technique compares the channel-sounder and VNA derived channel metrics from these measurements. Using mechanical switches, we established a controlled, static RF channel. The vector network analyzer has a comprehensive uncertainty analysis that propagates systematic and random uncertainties through to the power delay profiles. The method is suitable for millimeter-wave channel-sounder hardware with removable antennas.

**Index Terms**—channel-sounder verification, measurement uncertainty, millimeter-wave wireless communications, wireless system.

## I. INTRODUCTION

The future of the fifth-generation (5G) cellular communication lies with the millimeter-wave (mmWave) spectrum to meet the growing demand for greater capacity, denser networks, and lower latencies [1-5]. One fundamental challenge is the quantification of mmWave radio-propagation channels in a variety of environments and use scenarios: outdoor-to-indoor building penetration, highly-multipath, data backhaul, and other emerging scenarios. Characterization of this large variety of propagation channels and channel-model developments requires channel-sounders and a large body of skilled researchers. The 5G mmWave Channel Model Alliance [6] has been exchanging ideas, methodologies, and channel measurements between researchers from industry, academia, and government to characterize mmWave propagation channels and support innovative channel-model development.

As the technology for mmWave radio channel measurements becomes available, the use of channel-sounder verification is crucial for the characterization of the measurements of these mmWave RF channels. Hardware errors can come from the signal generation, up-conversion, amplification, signal reception, and down-conversion processes. As an example,

sampling circuits may introduce distortion, including quantization noise, nonlinearity, and imbalance (if interleaved) [7].

These hardware errors may propagate directly into the channel measurements, making it challenging to distinguish the actual channel response from hardware error even after calibration such as a back-to-back calibration. This can impact the estimation of the essential channel features and metrics such as power delay profile (PDP), frequency response, root-mean-square (RMS) delay spread, and path loss. Nonideal hardware combined with incorrect or inconsistent post-processing techniques may produce significant false artifacts in the estimated channel metrics, leading to potential erroneous mmWave channel models.

The success of the channel models for new mmWave scenarios depends significantly upon the accuracy and precision of the channel sounding measurements. By verifying the channel-sounder performance [8-9], we can determine the optimum channel-sounder system configuration, determine the significance of nonideal hardware and verify proper implementation of data post-processing. Many types of verification techniques exist to aid in understanding the capabilities of diverse types of channel-sounders.

One verification technique known as “*in-situ*” verification [10-13] uses the known measurement site for comparison of measured results to a simple analytical model like the Friis formula, a two-ray propagation model, or a ray-tracing simulation. The challenges with “*in-situ*” verification stem primarily from inaccurate assumptions in the model (i.e., the reflective properties of the environment) to inaccuracy in the system location and the antenna characteristics.

“Controlled condition” verification techniques use more controlled propagation conditions [14-18] such as anechoic chambers, conducted-cable measurements, or a well-controlled laboratory setting. Channel-sounder measured results are compared to analytic or ray-tracing models.

A third verification technique, known as “comparison-to-reference,” is based on the reference characterization of an unknown static channel with a calibrated vector network analyzer (VNA). Measurements conducted with the unknown channel-sounder are then compared to the reference

measurements. In [19], we described a conducted-channel portable verification artifact consisting of reconfigurable coaxial cables in a temperature-controlled box. This box supplies several different multipath channels pre-characterized by a VNA. Besides the static-channel requirement, there are no assumptions made about the propagation channel. The VNA captures intricate channel details such as multipath scattering from components or switches in the box as opposed to using a nominal ideal channel for comparison. A key feature of this approach is that the VNA measurements can be configured to reproduce the bandwidth and filtering of the unknown channel-sounder in order to compare the channel metrics. In the present work, we extend the technique to over-the-air channels and a higher frequency range by use of a highly-controlled, static, and open laboratory with demonstration using an E-Band correlation-based channel-sounder. Real-world propagation effects ie. spherical wave expansion exists in this approach, giving researchers similar measurement campaign conditions to verify their channel sounder performance.

As with the portable verification artifact approach, the comparison-to-reference verification presented here compares the channel-sounder measurements to VNA measurements having a comprehensive uncertainty analysis. We use mechanical switches to connect the VNA and a correlation-based channel-sounder to the radiating antennas as seen in Fig. 1. These switches help in meeting the controlled propagation condition and facilitate shifting the VNA's reference plane to the channel-sounder reference plane in post-processing such that both instruments effectively measure the same channel. To correctly shift the reference plan, we measured the components in the channel-sounder verification set-up such as the switches, waveguide sections, cables, and attenuators. Finally, this method applies to sounders with detachable antennas.

## II. COMPARISON-TO-REFERENCE CHANNEL-SOUNDER VERIFICATION

### A. Overview

We compare measurements made by the channel-sounder to those from a VNA. The uncertainty analysis makes use of the NIST Microwave Uncertainty Framework. This framework [20, 21] propagates random and systematic components of

uncertainties in the scattering-parameter measurements to the PDP and final resulting channel metrics such as RMS delay spread.

Mechanical waveguide switches minimize movement and the effects of reflection due to interface changes between the VNA and the channel-sounder measurements of the different controlled RF channels. We shift the VNA reference plane to the channel-sounder reference plane during the post-processing. With this step, the VNA and the channel-sounder measure the same controlled propagation channel and allows for a rigorous comparison of the channel metrics. To emulate a realistic (albeit static) mmWave RF channel, the controlled RF channel in the present work includes a direct path, multiple reflections, and other higher-order scattering paths.

The variable,  $h_{CS}(\tau)$ , denotes the complex impulse response of the controlled RF channel measured by the channel-sounder [22]. The *PDP* characterizes the received power as a function of time delay. We compute the channel-sounder measurements *PDP* from the magnitude squared of the channel impulse response as

$$PDP_{CS}(\tau) = |h_{CS}(\tau)|^2. \quad (1)$$

Next, we compute the magnitude of the complex channel impulse response for the VNA measurement,  $h_{VNA}(\tau)$ , from the average of  $S_{12}$  and  $S_{21}$ , (assuming the channel is reciprocal) as

$$|h_{VNA}(\tau)| = \left| IFFT \left( \frac{S_{12}(f) + S_{21}(f)}{2} \right) \right|. \quad (2)$$

The derived *PDP* from the VNA measurements is

$$PDP_{VNA}(\tau) = |h_{VNA}(\tau)|^2. \quad (3)$$

We derive channel metrics from the PDPs using ITU Radio Communication (ITU-R) P. 1407-5 [23]. These channel metrics are initial time of arrival, RMS delay spread, 90% delay window, noise threshold, and delay interval. Fig. 2 provides a graphical representation of these channel metrics.

### B. Measurement Set-up

Fig. 1 shows the set-up for the comparison-to-reference channel-sounder verification. We placed the channel-sounder

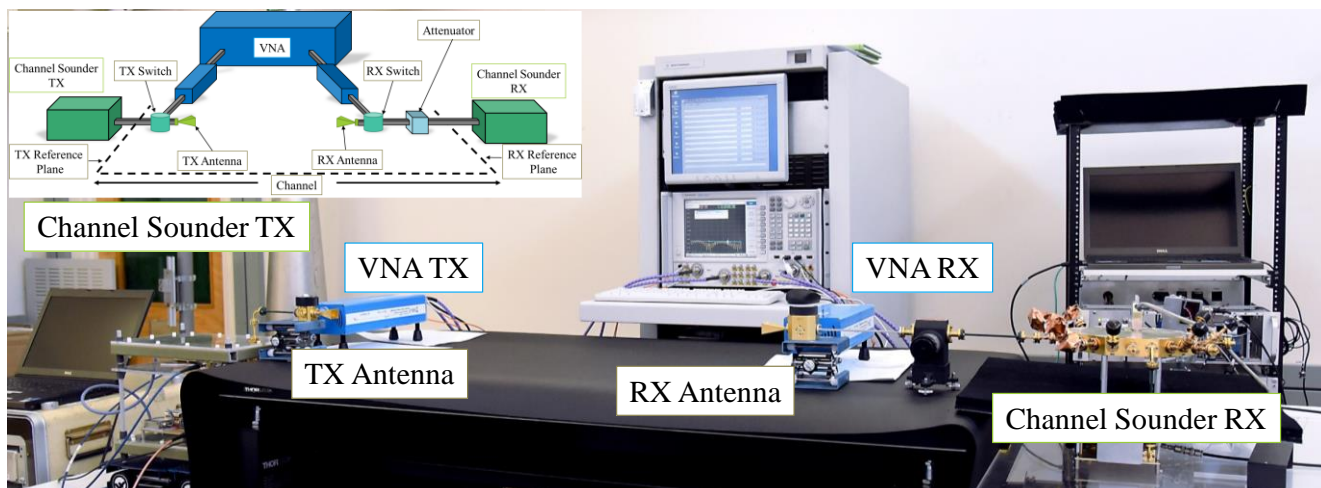


Fig. 1. Comparison-to-reference channel-sounder verification measurement set-up and schematic.

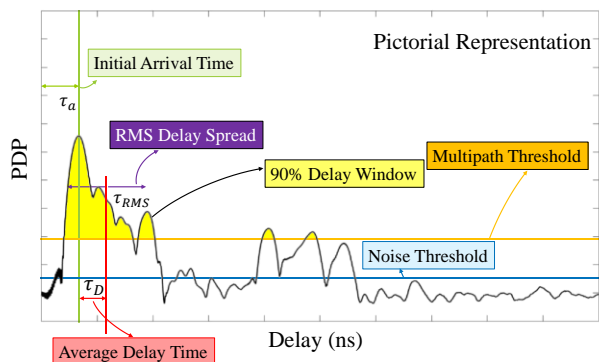


Fig. 2. Graphical representation of channel sounder metrics [22].

transmitter and receiver at opposite ends of an optical table, while the VNA was directly behind the optical table. The placement of the mechanical switches enabled easy access to both systems. Straight waveguide sections in the controlled RF channel connects the channel-sounder to the mechanical switches and an attenuator. This attenuator protects the channel-sounder’s receiver from potential exposure to high power. Before the measurement campaign, we characterized all waveguide sections, attenuators, and switches to ensure high-precision comparison. The antennas were scalar-feed horns with a half-power beamwidth of  $45^\circ$  in both vertical and horizontal planes [24]. The horns were vertically oriented during the tests.

### C. Uncertainty Analysis using the NIST Microwave Uncertainty Framework

The comparison-to-reference technique relies heavily on the VNA measurement components of uncertainty analysis. Ideally, the channel-sounder’s measured result would include an uncertainty analysis whose confidence bounds would fall within that of the reference measurement. Even without an uncertainty analysis, this comparison-to-reference technique provides independent, qualitative insight into the channel-sounder’s capabilities.

As mentioned above, the PDPs derived from the VNA measurements have both systematic and random components of uncertainties. The systematic components of uncertainty such as the mechanical standards are captured using models of these standards. These calibration models are incorporated into the Microwave Uncertainty Framework. Next, we assign uncertainties and probability distributions based upon the manufacturer specifications. Using this framework, we tracked correlations in uncertainties between calibration artifacts and between measured frequencies. Repeat measurements captured the random components of uncertainties such as receiver noise, system drift and switch repeatability.

We analyzed the uncertainties using both a sensitivity and Monte Carlo uncertainty analyses. The sensitivity analysis assumes Gaussian-distributed components of uncertainty and a linear uncertainty equation. The Monte Carlo uncertainty analysis accommodates non-Gaussian probability distributions, propagates uncertainties through the nonlinear measurement equations, detects statistical bias in the results, and checks assumptions such as linearity of the sensitivity analysis. These analyses propagate the uncertainties from the VNA scattering

parameters to the channel metrics in Fig. 2.

### D. Controlled RF Channels

In conjunction with the uncertainty analysis, the comparison-to-reference channel-sounder verification process requires a controlled RF channel. This channel must be stable and repeatable, with as little movement in the cables as possible, little difference in the propagation channel, and no change to the interface reflections during both the VNA and channel-sounder measurements. The measurement campaign should have a stable humidity and temperature set by a temperature controller due to the sensitivity of the measurement instruments in the mmWave operating region. To limit potential fast-fading multipath sources, we reduced environmental movement by limiting personnel access to the laboratory.

This study used three controlled test channels, as shown in Fig. 3. The first test channel was a direct line-of-sight (LOS) channel. The antenna separation is not critical as long as it is held constant throughout the entire measurement sequence. In the second test channel, we pointed the antennas toward one another at approximately 1.0-meter separation (no change from the first reference channel) with the addition of two highly conducting metal sheets (termed “MS-LOS”), placed behind the channel-sounder’s TX and RX antennas. The metal sheets had a 1.6-meter separation. The third test channel was a non-line-of-sight (nLOS) channel. For this channel, the antennas were placed parallel to one another and pointed toward a far wall in the laboratory.

Because the channel-sounder and VNA reference planes are at waveguide interfaces, the controlled RF channel includes the effects of the antenna radiation pattern and antenna gain. If the

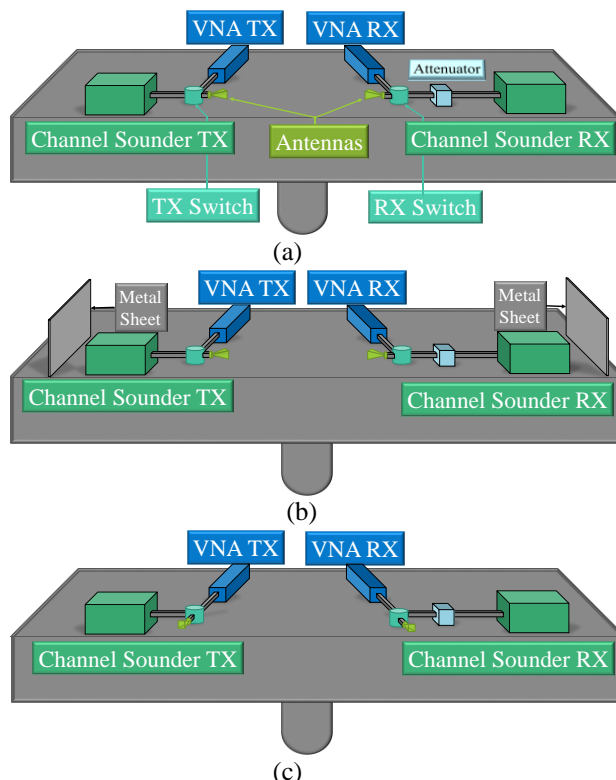


Fig. 3. Controlled test channels: (a) LOS, (b) MS-LOS, (c) nLOS.

channel is static (i.e. the antenna does not move) the antenna variation between the VNA and channel-sounder is minimized.

Another consideration is the choice of antenna separation. A 1-meter separation for the LOS test channel ensured both far-field propagation and a measured signal that was well above the system noise floor. For the MS-LOS channel, a separation of 1.6-meters between the metal plates gives strong multiple reflections in addition to the direct path in the PDP. Finally, we select the antenna separation and orientation for the nLOS test channel to stay outside of either antenna’s main beam.

E. Mechanical Switches

The WR-10 mechanical switches, as seen in Fig. 4, enable a stable, repeatable, and controlled propagation channel. We minimized changes in the internal hardware reflections during the measurements using these switches. The switch eliminates the need to connect and disconnect the VNA and the channel-sounder to the auxiliary equipment. Also, since there is little physical movement of the hardware, there is little concern that the antenna may move during the measurements.

III. IMPLEMENTATION AND PROCESSING

A flowchart illustrating the comparison-to-reference verification technique is shown in Fig. 5. The process uses the pre-measured switches to shift the VNA reference planes to the channel-sounder reference planes. Repeat measurements support the uncertainty analysis. “Before” and “after” calibrations of the VNA capture any changes in the VNA system or cables. Post-processing is used for calculation of the channel metrics.

A. Identify and Choose Controlled RF Channels

The first step in the channel-sounder verification process is the identification of the test channels that provide controlled, stable RF channel conditions. As discussed earlier, these are LOS, MS-LOS, and nLOS test channels.

B. Establish software and hardware settings

The channel-sounder software and hardware settings used in the verification measurement should be the same settings used during a channel-sounder measurement campaign. An important part of the comparison is that the VNA software and hardware settings reproduce the intended bandwidth and filtering of the channel-sounder in hardware or post-processing. For the comparison considered here, the IF bandwidth of the VNA was set to 10 Hz to achieve a high dynamic range. Next, the channel-sounder frequency range determined the VNA frequency range. A dwell time equaled 1 ms to settle the VNA system. Finally, we determined the number of points,  $N_{VNA}$ , for the VNA based upon the channel-sounder parameters as follows. First, the VNA frequency-domain measurements were converted to the time-domain. The time resolution,  $\Delta T_{VNA}$ , of the VNA is dependent upon the VNA frequency range,  $F_R$

$$\Delta T_{VNA} = 1/F_R \tag{4}$$

The maximum VNA observable time,  $T_{max}^{VNA}$ , is

$$T_{max}^{VNA} = N_{VNA} \Delta T_{VNA}, \tag{5}$$

where  $N_{VNA}$  is the number of VNA data points. To determine  $N_{VNA}$ , we set the VNA maximum observable time,  $T_{max}^{VNA}$ , to the channel-sounder maximum observable time,  $T_{max}^{CS}$ . The computation of the number of VNA data points is

$$N_{VNA} = T_{max}^{CS} / \Delta T_{VNA} \tag{6}$$

C. Measure Hardware Components Scattering-Parameters

Next, as shown in the flow chart, are the VNA scattering-parameter measurements of the mechanical switch paths, attenuators, and waveguides. We measure the switches to shift the VNA reference plane to the channel-sounder reference plane. Fig. 6 provide a schematic of the paths through the TX and RX switches.

D. Connect CS and VNA Hardware to the Switches

We typically calibrate the VNA using WR-10 waveguide short, offset shorts, load, and thru calibration standards. The calibration kit models used the calibration kit’s standards, including flange misalignment for our uncertainty analysis. Once calibrated, the VNA is connected to the mechanical switches in the configuration shown in Fig. 1.

A Back-to-Back (B2B) calibration [25] was performed on the channel-sounder before the measurements. For illustrative purposes, we applied two different types of calibrations to the E-band channel-sounder’s measured data of the channel. The

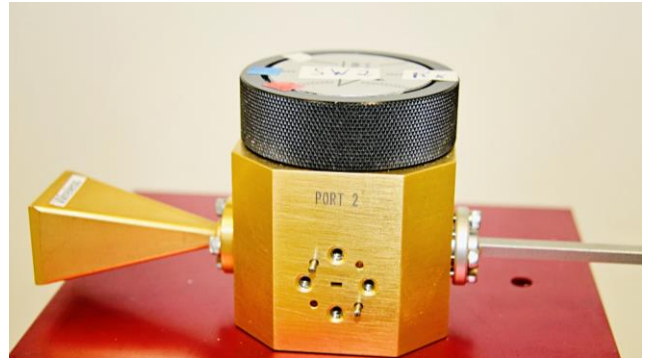


Fig. 4. Mechanical waveguide switches used in the measurements.

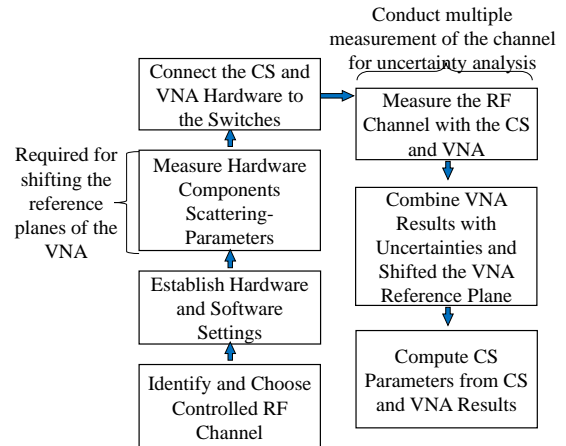


Fig. 5. Flowchart of comparison-to-reference channel-sounder (CS) verification process.

first calibration technique, termed “Scalar B2B” used a power meter to correct for the power offset between the known power loss in an attenuator and the raw channel measurement. The second calibration technique, termed “Vector B2B”, applied a complex-valued correction to the channel-sounder measurements of a channel. The measured channel impulse response (CIR) via a B2B channel is compared with an ideal pseudorandom sequence. The difference is used to calibrate the PDPs collected in the field. This “Vector B2B” method is also termed as post-processing filters, please refer [26]-[28] for details. Both techniques were applied in post-processing.

**E. Measure RF Channel with CS and VNA**

First, the channel-sounder repeatedly measured the test channel for five minutes, collecting 81,880 measurements. Due to local oscillator (LO) drift at the time of the measurement, the results presented here are based on a single measurement to produce the PDPs, since averaging of the channel-sounder measurements gave incorrect results. These points to a potential problem in the channel-sounder architecture. Next, the rotation of the switches connected the VNA to the test channel. The VNA measured each test channel ten times. Due to the low IF bandwidth, this set of ten measurements took about eight hours to complete. These measurements determined the repeatability for the uncertainty analysis. To study reproducibility, we repeated this sequence for each test channel for two days for a total of 20 VNA measurements for each test channel.

**F. Combine VNA Results with Uncertainties and Shifted the VNA Reference Plane**

After the completion of the measurements and before the channel-sounder comparison, we averaged the VNA measurements and, as illustrated in Fig. 6, shifted the VNA reference planes to the channel-sounder reference planes. Both were accomplished using the Microwave Uncertainty Framework.

We shifted the VNA’s reference plane by cascading the scattering-parameter matrices for the VNA’s calibration error terms with the measured scattering-parameter matrices for the switches and other structures between the channel-sounder reference planes and the VNA reference planes. All components between these two reference planes, including the waveguides, attenuators, and controlled RF channel, were considered to be part of the channel, as shown in Fig. 1.

**G. Compute CS Parameters from CS and VNA Results**

After shifting the reference planes of the VNA

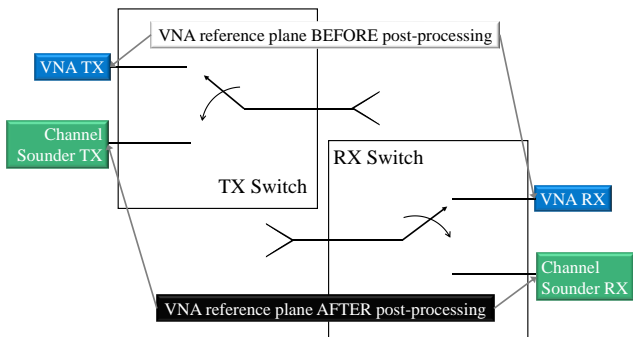


Fig. 6. Measurement paths for the mechanical switch

measurements, one final step before the comparison is to apply the channel-sounder filter to the VNA measurements. This step may or may not need to be implemented depending upon the channel-sounder post-processing. The correlation-based channel-sounder post-processing approach uses a match-filter to remove the amplified noise at the band edges [27]. The filter consists of the oversampled pseudorandom noise (PN) sequence transmitted signal [22]. The filter is a magnitude-square of the Fourier transform of the PN sequence, which is a sinc-squared function with a null-to-null bandwidth of 2 GHz. The length of the PN sequence is 2047 bits. We applied this filter to the VNA measurements.

Fig. 7(a) shows the PDP results from the channel-sounder and VNA without the filter for an nLOS channel and Fig. 7(b) shows the same results but now with the filter applied to the VNA measurements. There is a better agreement between the VNA measurements with the filter than without the filter. This example illustrates that the choice of filtering is critical due to its impact on the channel metrics derived from measured results. That is, post-processing differences can impede comparison of hardware performance. The following figures show the VNA PDP (VNA: Nominal) and the standard uncertainty (VNA: Std. Unc.).

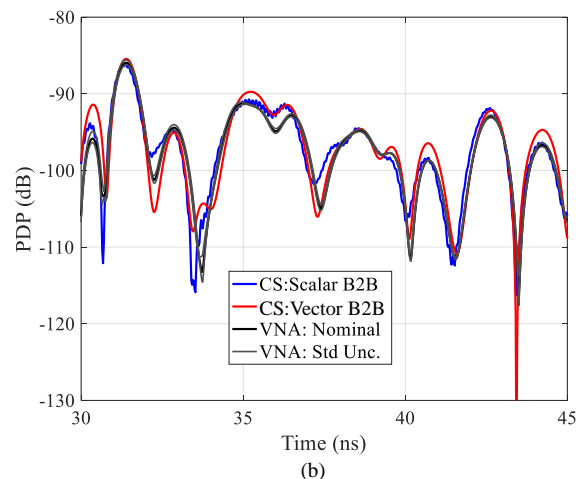
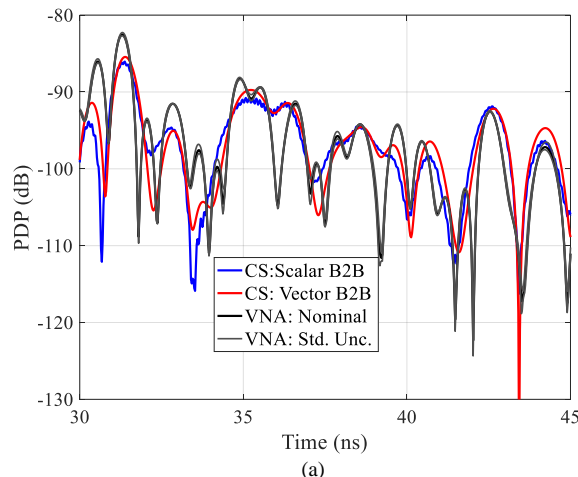


Fig. 7. Scaled PDP for a nLOS test channel: (a) without a filter and (b) with a filter.

Upon completion of this task, we computed multiple channel metrics such as PDPs, RMS delay spread, delay window, and number of multipath components.

#### IV. MEASUREMENT COMPARISON

The final step in the channel-sounder verification process is the comparison of the PDPs and key channel metrics. A comparison of the VNA- and channel-sounder-derived PDPs used the LOS test channel, is shown in Fig. 8. We applied the filter and a power normalization known as “area scaling” to all channel-sounder and VNA PDPs. Area scaling integrates the PDP over time to approximate the path gain of the channel [26]. We time aligned the initial time of arrival of the signal of the channel-sounder PDPs to the VNA’s initial arrival time in the figures below. The initial time of arrival and the initial power level for LOS and nLOS test channels is given in Table I. While the TX and RX antenna separation distance is approximately 1.0 m, the systems’ reference planes, as shown in Fig. 1, include additional waveguide lengths and hardware components along with the 1.0-m length. The VNA accurately captures this additional length. Table I lists the initial power levels at the time of arrival. The initial power level of the channel-sounder falls outside of the VNA’s measurement uncertainty.

Further inspection of Fig. 8(a) shows multiple pulses and ripples in the channel-sounder-derived PDP that are not in the VNA-derived PDP. The first of these pulses arrives at 7.63 ns with a power level that is 27 dB below the initial peak power level. Therefore, the RMS delay spreads in Table II, created with a multipath threshold (Mth) of 20 dB, are comparable with a difference of only 0.01 ns between the VNA and the CS. As the multipath threshold increases, the difference between the channel metrics derived from the two systems also increases. Note that the CS number of multipath components at a multipath threshold of  $-50$  dB is seven more than the VNA results. The table contains the delay windows as well. Depending on the multipath threshold used in channel-model development, these differences may or may not be significant.

In Fig. 8(b), the channel-sounder PDP level beyond 40 ns is larger than that of the VNA. The channel-sounder has a value of  $-110$  dB around 100 ns while the VNA value is  $-140$  dB as seen in Fig. 8(b).

Next, we compared the PDPs for the MS-LOS test channel. The channel-sounder results, shown in Fig. 9, processed to the initial time of arrival of the VNA of 6.38 ns. After this shift, in Fig. 9(a), we see that the first multipath pulse arrives at 18.1 ns for both systems, with a power-level difference of  $2 \text{ dB} \pm 0.13 \text{ dB}$  between the VNA and both channel-sounder calibration techniques. Closer inspection of the first multipath pulse in Fig. 9 shows a rippling and a slant in the bell shape curve in the ‘CS: Scalar B2B’ versus the VNA result and the ‘CS: Vector B2B’ result. This distortion leads to deviation in the power levels for other multipath peaks with quantification of these deviations by using the channel metrics, as seen in Table III.

As seen in Fig. 9(b), the channel-sounder-derived PDP level at around 100 ns of approximately  $-115$  dB is higher than the VNA-derived PDP level of  $-130$  dB, indicating a higher noise floor for the channel-sounder.

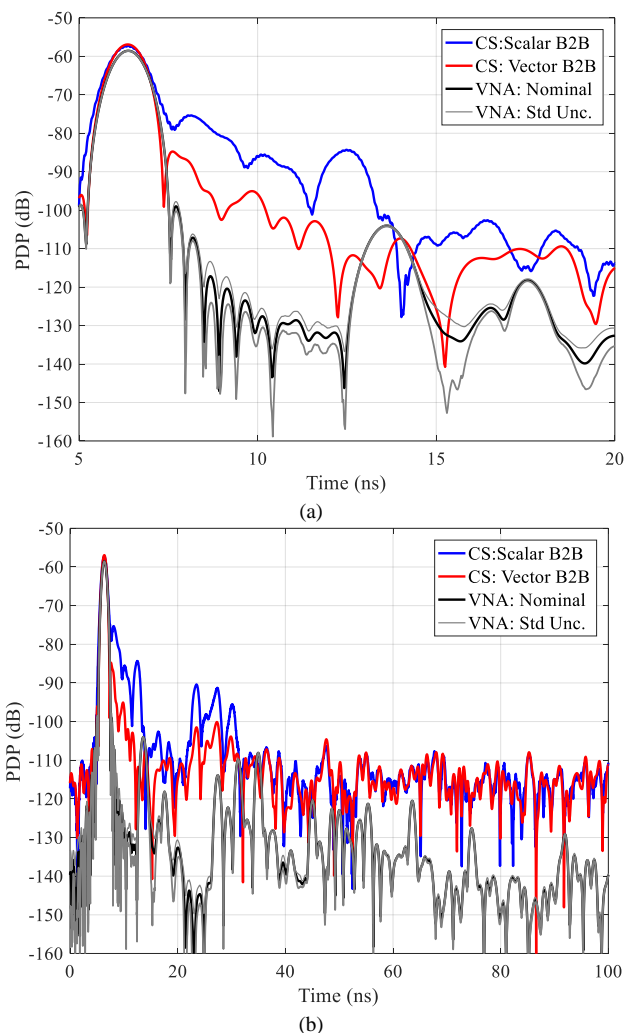


Fig. 8. Scaled PDP for the LOS test channel: (a) zoomed-in and (b) extended to 100 ns.

The last comparison of the PDPs is for the nLOS test channel. Once again, we applied the filter to the VNA measurements and time-shifted the channel-sounder results, shown in Fig. 10, to the initial time of arrival of the VNA of 31.38 ns. The VNA- and channel-sounder-derived PDPs show similar time responses, which is supported by the RMS delay spread for ‘CS: Vector B2B’ but not for the ‘CS: Scalar B2B’ in Table IV.

Table I  
CHANNEL SOUNDER (CS) PARAMETER COMPARISON

(a) LOS test channel with multipath threshold of -20 dB		
	Arrival Time (ns)	Initial Power Level (dB)
NIST VNA	6.38	$-58.56 \pm 0.09$
CS: Vector B2B	3.16	-56.92
CS: Scalar B2B	3.33	-57.21
(b) nLOS test channel with multipath threshold of -20 dB		
	Arrival Time (ns)	Initial Power Level (dB)
NIST VNA	31.38	$-85.95 \pm 0.37$
CS: Vector B2B	3.11	-85.44
CS: Scalar B2B	3.33	-86.04

The conclusions that may be drawn on the capability of the

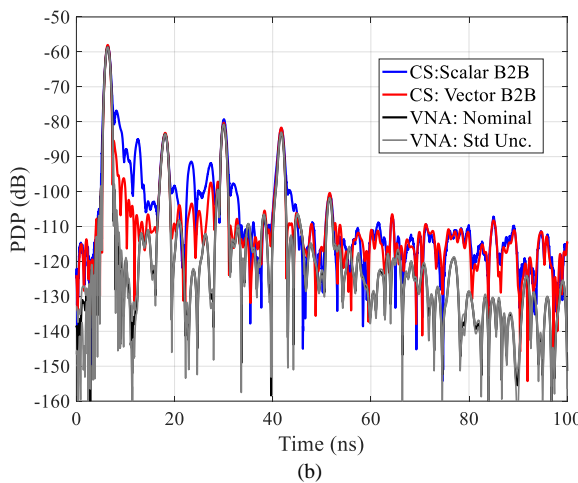
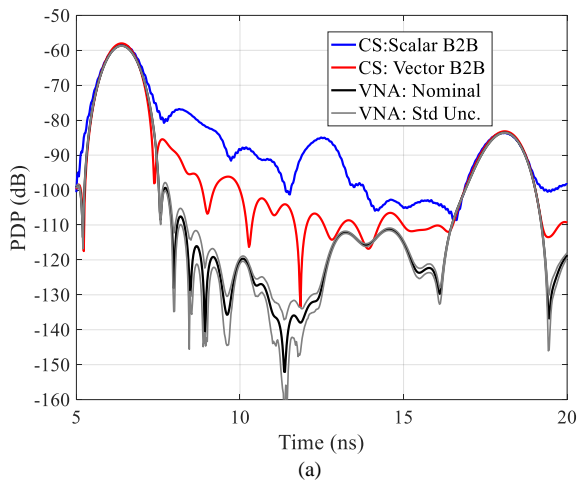


Fig. 9. Scaled PDP for the MS-LOS test channel: (a) zoomed in, and (b) extended to 100 ns.

Table II  
LOS CHANNEL METRICS COMPARISON

		RMS Delay spread (ns)	Delay Window (ns)	Number of Multipath Components
Mth = -10 dB	VNA	$0.29 \pm 0$	$1.09 \pm 0$	1
	CS: Vector B2B	0.28	1.05	1
	CS: Scalar B2B	0.31	1.35	1
Mth = -20 dB	VNA	$0.31 \pm 0$	$1.09 \pm 0$	1
	CS: Vector B2B	0.3	1.05	1
	CS: Scalar B2B	0.38	1.35	2
Mth = -30 dB	VNA	$2.74 \pm 0.05$	$1.09 \pm 0$	4
	CS: Vector B2B	2.95	1.05	5
	CS: Scalar B2B	3.12	1.35	8
Mth = -40 dB	VNA	$2.86 \pm 0.05$	$1.09 \pm 0$	5
	CS: Vector B2B	3.07	1.05	8
	CS: Scalar B2B	3.31	1.35	11
Mth = -50 dB	VNA	$2.9 \pm 0.05$	$1.09 \pm 0$	11
	CS: Vector B2B	3.11	1.05	18
	CS: Scalar B2B	3.38	1.35	18

Table III  
MS-LOS CHANNEL METRICS

		RMS Delay spread (ns)	Delay Window (ns)	Number of Multipath Components
Mth = -10 dB	VNA	$0.29 \pm 0$	$1.09 \pm 0$	1
	CS: Vector B2B	0.28	1.05	1
	CS: Scalar B2B	0.31	1.35	1
Mth = -20 dB	VNA	$0.31 \pm 0$	$1.09 \pm 0$	1
	CS: Vector B2B	0.3	1.05	1
	CS: Scalar B2B	0.38	1.35	2
Mth = -30 dB	VNA	$2.74 \pm 0.05$	$1.09 \pm 0$	4
	CS: Vector B2B	2.95	1.05	5
	CS: Scalar B2B	3.12	1.35	8
Mth = -40 dB	VNA	$2.86 \pm 0.05$	$1.09 \pm 0$	5
	CS: Vector B2B	3.07	1.05	8
	CS: Scalar B2B	3.31	1.35	11
Mth = -50 dB	VNA	$2.9 \pm 0.05$	$1.09 \pm 0$	11
	CS: Vector B2B	3.11	1.05	18
	CS: Scalar B2B	3.38	1.35	18

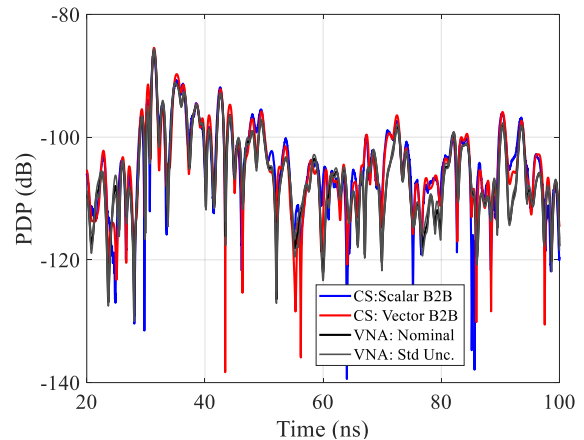


Fig. 10: Scaled PDP vs. time for the nLOS test channel extended to 100 ns.

Table IV  
nLOS channel metrics comparison with filtering.

		RMS Delay spread (ns)	Delay Window (ns)	Number of Multipath Components
Mth = -10 dB	VNA	$3.45 \pm 0.12$	$59.63 \pm 3.06$	6
	CS: Vector B2B	3.36	35.3	5
	CS: Scalar B2B	3.43	35.91	5
Mth = -20 dB	VNA	$16.58 \pm 0.9$	$59.63 \pm 3.06$	22
	CS: Vector B2B	8.9	35.3	19
	CS: Scalar B2B	9.48	35.91	18

channel-sounder as compared to the VNA reference system require keeping in mind that the channel-sounder performance is often highly dependent on the desired measurement conditions. Therefore, the reference-to-comparison technique described here provides a quantifiable approach to determine

the level of attainable accuracy desired for specific measurement conditions. Understanding this issue is key to the correct use of the channel-sounder. For example, the Vector B2B is clearly a more suitable back-to-back technique than the Scalar B2B for this channel-sounder.

## V. CONCLUSIONS

We presented a comparison-to-reference channel-sounder verification technique to assess a channel-sounder's performance in a static, over-the-air test environment at mmWave frequencies. The method is based on a static RF channel with mechanical switches and a reference VNA. The reference VNA measures three different test channels, followed by a measurement of the same channel with the channel-sounder. We shifted the VNA measurement reference planes to the channel-sounder reference planes. The VNA can provide traceability through the calibration standards. The VNA PDPs and other channel metrics have both systematic and random components of uncertainties. The work presented here illustrated comparison measurements for three different test channels.

The comparison-to-reference technique provides a unique approach that does not require as many assumptions about the environment or artifacts compared to many simulated-channel verification techniques. Also, by matching the post-processing characteristics between the two instruments, this technique can isolate non-ideal hardware effects that may produce false pulses or other distortions in the PDPs. Channel metrics often interpret these false pulses as multipath components. Thus, the comparison-to-reference technique provides insight into a channel-sounder's performance when its data are used for calculating PDPs and channel metrics.

## ACKNOWLEDGMENT

The work presented here was performed in collaboration with NIST colleagues Camillo Gentile and Nada Golmie.

## REFERENCES

- [1] The Institute of Electrical and Electronics Engineers (IEEE) Future Networks Initiative, Online: <https://5g.ieee.org/>, accessed June 08, 2020.
- [2] 3GPP, "Technical specification group radio access network; Study on channel model for frequencies from 0.5 to 100 GHz (Release 15)," 3rd Generation Partnership Project (3GPP), TR 38.901 V15.0.0, June 2018. Online: <http://www.3gpp.org/DynaReport/38901.htm>, accessed June 08, 2020.
- [3] The 5G Infrastructure Public-Private Partnership (5G-PPP). Online: <https://5g-ppp.eu/>, accessed June 08, 2020.
- [4] 5G Forum, Online: <https://ieee-wf-5g.org/>, accessed June 08, 2020.
- [5] J. Lee *et al.*, "Spectrum for 5G: Global Status, Challenges, and Enabling Technologies," in *IEEE Communications Magazine*, vol. 56, no. 3, pp. 12-18, March 2018, doi: 10.1109/MCOM.2018.1700818.
- [6] 5G mmWave Channel Model Alliance Wiki Website, <https://sites.google.com/a/corneralliance.com/5g-mmwave-channel-model-alliance-wiki/home>
- [7] K. A. Remley, D. F. Williams, P. D. Hale, C-M Wang, J. A. Jargon, and Y. Park, "Millimeter-wave modulated-signal and error-vector-magnitude measurement with uncertainty," *IEEE Trans. MTT*, vol. 63, no. 5, pp. 1710-1720, May 2015.
- [8] J. Quimby, D. G. Michelson, M. Bennai, K. A. Remley, J. Kast and A. Weiss, "Interlaboratory Millimeter-Wave Channel-sounder Verification," *2019 13th European Conference on Antennas and Propagation (EuCAP)*, Krakow, Poland, 2019, pp. 1-5.
- [9] K. A. Remley, C. Gentile, A. Zajic and J. T. Quimby, "Methods for Channel-sounder Measurement Verification," *2017 IEEE 86th Vehicular Technology Conference (VTC-Fall)*, Toronto, ON, 2017, pp. 1-4.
- [10] G. R. MacCartney, Jr. and T. S. Rappaport, "A flexible millimeter-wave channel-sounder with absolute timing," *IEEE Journal on Selected Areas in Communications*, vol. 35, no. 6, pp. 1402-1418, June 2017.
- [11] G. R. MacCartney, Jr. and T. S. Rappaport, "A flexible wideband millimeter-wave channel-sounder with local area and NLOS to LOS transition measurements," *2017 IEEE International Conference on Communications (ICC)*, Paris, France, May 2017, pp. 1-7.
- [12] C. Cheng, S. Kim and A. Zajic, "Comparison of path loss models for indoor 30 GHz, 140 GHz, and 300 GHz channels," *2017 11th European Conference on Antennas and Propagation (EuCAP)*, Paris, 2017, pp. 716-720.
- [13] A. Karstensen, W. Fan, I. Carton, G. F. Pedersen, "Comparison of ray tracing simulation and channel measurements at mmWave bands for indoor scenarios," *EuCAP*, 2016, pp. 1-5.
- [14] J. Quimby, J. Jargon, R. Leonhardt, P. Hale, K. A. Remley, A. Koepke, S. Street, R. Johnk, C. Hammerschmidt, P. McKenna, I. Strange, N. DeMinco, J. Diener, J. Rezac, R. "Chad" Smith, C. Hoyt, and S. Springer, "Channel-sounder Measurement Verification: Conducted Tests" Technical Note (NIST TN), TN 2076, April 15, 2020.
- [15] Y. Xing, O. Kanhere, S. Ju, T. S. Rappaport and G. R. MacCartney, "Verification and Calibration of Antenna Cross-Polarization Discrimination and Penetration Loss for Millimeter Wave Communications," *2018 IEEE 88th Vehicular Technology Conference (VTC-Fall)*, Chicago, IL, USA, 2018, pp. 1-6, doi: 10.1109/VTCFall.2018.8690683.
- [16] C. U. Bas *et al.*, "Real-Time Millimeter-Wave MIMO Channel-sounder for Dynamic Directional Measurements," in *IEEE Transactions on Vehicular Technology*, vol. 68, no. 9, pp. 8775-8789, Sept. 2019, doi: 10.1109/TVT.2019.2928341.
- [17] D. He, B. Ai, K. Guan, L. Wang, Z. Zhong and T. Kürner, "The Design and Applications of High-Performance Ray-Tracing Simulation Platform for 5G and Beyond Wireless Communications: A Tutorial," in *IEEE Communications Surveys & Tutorials*, vol. 21, no. 1, pp. 10-27, Firstquarter 2019, doi: 10.1109/COMST.2018.2865724.
- [18] S. Salous, S. Feeney, X. Raimundo, and A. Cheema, "Wideband MIMO channel-sounder for radio measurements in the 60 GHz band," *IEEE Trans. Wireless Commun.*, vol. 15, no. 4, pp. 2825-2832, Apr. 2016.
- [19] J. N. H. Dortmans, J. T. Quimby, K. A. Remley, D. F. Williams, J. Senic and R. Sun, "Design of a Portable Verification Artifact for Millimeter-Wave-Frequency Channel-sounders," in *IEEE Transactions on Antennas and Propagation*, vol. 67, no. 9, pp. 6149-6158, Sept. 2019, doi: 10.1109/TAP.2019.2902623.
- [20] D. F. Williams, J. C. M. Wang, and U. Arz, "An optimal vector-network-analyzer calibration algorithm," *IEEE Trans. MTT*, vol. 51, no. 12, pp. 2391-2401, Dec. 2003.
- [21] National Institute of Standards and Technology On-Wafer Calibration Software, Online: <https://www.nist.gov/services-resources/software/wafer-calibration-software>, accessed Apr 05, 2019
- [22] J. Quimby, R. Candell, K. A. Remley, D. Novotny, J. Diener, P. Papazian, A. Curtin, G. Koepke, "NIST Channel-sounder Overview and Channel Measurements in Manufacturing Facilities," NIST Technical Note, TN 1979.
- [23] ITU Radio Communication (ITU-R) P. 1407-5, 2013.
- [24] Josh Gordon, David Novotny, "High-Tech Measurements for High Frequency Antennas", [http://www.nist.gov/ct/rftechnology/rf\\_fields/robot-arm-aids-antenna-calibration.cfm](http://www.nist.gov/ct/rftechnology/rf_fields/robot-arm-aids-antenna-calibration.cfm), accessed November 23, 2020.
- [25] S. Salous, Radio Propagation Measurement and Channel Modelling, Wiley 2013.
- [26] R. Sun, D. Williams, D. Novotny, C. Gentile, K.A. Remley, P. Papazian, J. Quimby, A. Curtin, "Power delay profile calibration and comparison techniques for microwave and millimeter-wave channel-sounder," In progress.
- [27] R. Sun, P. B. Papazian, J. Senic, Y. Lo, J. Choi, K. A. Remley, C. Gentile, "Design and Calibration of a Double-directional 60 GHz Channel Sounder for Multipath Component Tracking," *11th European Conference on Antennas and Propagation (EuCAP 2017)*, pp. 3336-3340, Paris, France, 19-24 Mar. 2017.
- [28] P. B. Papazian, J. Choi, J. Senic, P. Jeavons, C. Gentile, N. Golmie, R. Sun, D. Novotny, K. A. Remley, "Calibration of millimeter-wave channel sounders for super-resolution multipath component extraction," *2016 10th*

*European Conference on Antennas and Propagation (EuCAP)* , pp. 1-5,  
Davos, Switzerland, 2016.